Phase diagram of the unconventional superconductor UPt_3 in the weak-crystal-field model

M. E. Zhitomirsky
Institute for Solid State Physics, University of Tokyo, Tokyo 106, Japan
and L. D. Landau Institute for Theoretical Physics, Moscow, 117334, Russia

Kazuo Ueda
Institute for Solid State Physics, University of Tokyo, Tokyo 106, Japan
(Received 26 June 1995)

We study the phase diagram of the heavy fermion superconductor UPt_3 within a phenomenological model with two nearly degenerate order parameters corresponding to the A_1 and E_1 irreducible representations. A weak effect on superconductivity from the crystal lattice is also assumed. This assumption on one side provides an explanation for the closeness of two critical temperatures. On the other side it yields parameters of the Ginzburg-Landau functional which lead to a single superconducting transition when the order of critical temperatures changes with pressure. The experimental H-T diagram with a tetracritical point is reconstructed in the AE model. Vortex lattices are found for two orientations of the field. Restrictions imposed on the theory of the UPt_3 phase diagram by experiments at pressures above critical and in a tilted magnetic field are also discussed.

I. INTRODUCTION

The most convincing evidence of an unconventional superconductivity in the heavy fermion compound UPt_3 is its complicated H-T diagram with multiple superconducting phases. The main features of this phase diagram are (i) a small (about 10%) splitting of the superconducting critical temperature $T_c \approx 0.5$ K in zero field and (ii) a tetracritical point coinciding with (iii) a kink in the temperature dependence of the upper critical field for two orientations of the magnetic field, parallel and perpendicular to the hexagonal c axis.[1] The assumption about anisotropic Cooper pairing in UPt_3 is also supported by various thermodynamic and transport measurements which are compatible with zeros in the energy gap below T_c.[1]

Despite this rich experimental information, no unambiguous identification of the symmetries of superconducting phases has been made to date. Let us discuss the pros and cons of various theoretical models of the UPt_3 phase diagram[2–15] in the light of recent experimental studies under uniaxial pressures[16] and tilted magnetic field.[17] Different interpretations of this phase diagram fall into two main classes. The first class of theories is so-called symmetry-breaking field (SBF) models. They assume a degenerate multicomponent superconducting order parameter (usually corresponding to a multidimensional irreducible representation of the D_{6h} point group) interacting with a weak additional field, which produces a small splitting of T_c. The degeneracy of the order parameter may be connected either with its orbital part[3,4] or with the spin part of the pairing function.[7] Two candidates for an intrinsic SBF in UPt_3 have been proposed:[2,9] an antiferromagnetic order with in-plane moments developed below $T_N \approx 5$ K (Ref. 18) or a macroscopic strain field due to incommensurate structural domains.[19] The former is considered as the primary SBF because it is suppressed by a hydrostatic pressure $P^* \sim 5.4 \pm 2.9$ kbar,[20] which is roughly of the same order as the critical pressure $P_{cr} \approx 3.8$ kbar for the disappearance of the double superconducting transition.[21] The difficulty in explaining the same topology of the phase diagram for different orientations of the field, which existed at the first versions of SBF models,[3,4] was solved by turning off the mixing gradient terms in the later variants.[7,11–13]

All models using antiferromagnetic order as SBF have, however, a common difficulty. As is known from neutron scattering experiments,[18] the tiny magnetic moments on U atoms are ordered antiferromagnetically with a very short correlation length $a \approx 150$ Å, which is comparable to the superconducting coherence length at zero temperature, $\xi_0 \approx 110$ Å.[22] In order to have a nearly isotropic H_{c2} in the basal plane[23] one should assume that the moments rotate freely, maintaining their perpendicular orientation with respect to the magnetic field. Even if this theoretical assumption is correct, a serious problem still exists for *zero-field* behaviors. Zero-field magnetic structure in UPt_3 consists of small domains with equivalent orientations of antiferromagnetic vectors in the hexagonal lattice.[20,24] As has been recently shown by Isaacs *et al.*[24] with the help of magnetic x-ray and neutron diffraction studies, this orientational disorder of magnetic moments is frozen at $H=0$. The appearence of superconductivity leads to a slight reduction of the magnitude of the staggered moments below T_c without changes in the symmetry. Under such conditions there are many chaotically oriented magnetic domains on the scale of the superconducting coherence length $\xi(T) \gg \xi_0, a$. This randomness in the orientation restores near T_c the average in-plane isotropy for the superconducting order parameter, and the usual scenario for the double transition, $(1,0) \rightarrow (1, i\alpha)$, proposed for homogeneous SBF,[2,3] does not work. The only realistic consideration taking into account the random domain structure was presented by Joynt *et al.*[6] They showed that though the double transition between nonhomogeneous "glass" and homogeneous superconducting phases is possible in this case, the second transition will be of first order, which is in

obvious contradiction with the existing experimental data.

Another weak point of these models independent of the nature of the SBF is the interpretation of the H-T diagram at uniaxial pressures above the critical value, where the splitting of T_c disappears. Boukhny *et al.*[16] found for several values of $P>P_{\rm cr}$ and both field orientations that the inner line of phase transitions inside the mixed state $H_{FL}(T)$ is not traced back to T_c, but intersects with the $H=0$ axis at some intermediate temperature T^*. They interpreted further the almost-temperature-independent line $T^*(P)$ as a missing fourth line of phase transitions in the P-T plane.[1,25] Though such behavior of the fourth boundary in the P-T plane may be explained by the temperature dependence of the critical pressure, which destroys the antiferromagnetic order, the behavior of the inner transition line in the mixed state (at constant pressure) does contradict the SBF concept. After the disappearance of the SBF with pressure, the degeneracy is restored and all components of the superconducting order parameter have the same critical temperature. Therefore, transition lines between various vortex structures[26–30] should originate from a single T_c for any $P>P_{\rm cr}$. The lack of enough accuracy in the experimental data[16] at the low-field region leaves a certain degree of ambiguity in the exact behavior of the inner line, but this observation makes SBF scenarios at least questionable.

An alternative phenomenological approach to the phase diagram of UPt_3 is to let critical temperatures of two different irreducible representations of the D_{6h} group to be close to each other. Such an assumption was used originally to describe the splitting of T_c in the other heavy fermion superconductor UBe_{13} under doping of Th impurities.[31] Two types of analogous models were elaborated for UPt_3 in Ref. 6 and one of them, the so-called AB model, was studied later in detail by Chen and Garg.[8] The disadvantage of this argument was realized soon after the experimental observation of the convergence rather than crossing of two specific heat anomalies in UPt_3 under pressure.[21] Generally, if the order of the critical temperatures for two independent irreducible representations changes, the splitting should reappear again after the intersection point. To explain thermodynamic measurements,[1] which did not show the split phase transition at $P>P_{\rm cr}$, one has to assume, in addition to the accidental degeneracy of critical temperatures, also an accidental relation of phenomenological constants describing the interaction of two order parameters in the Ginzburg-Landau (GL) functional. [In the AB model[8] the necessary condition for the disappearance of the T_c splitting after $P_{\rm cr}$ is $(\beta_a-\beta')/(\beta_b-\beta')\gg 1$.] Additional phenomenological parameters in gradient terms are introduced in such models[6,8] to obtain a kink in $H_{c2}(T)$ for both $H\perp c$ and $H\| c$ and so on. Explaining experiments, accidental degeneracy models fail to provide physical explanation for the choice of quite artificial parameter values and, therefore, raise a question:[32] Is it possible that accidental features of the GL functional reflect a hitherto unidentified symmetry of the superconducting order parameter in UPt_3.

Semimicroscopic theories for the superconducting order parameter in UPt_3, which use an exchange of spin fluctuations as a mean of pairing, yield, for example, close critical temperatures for either the pair of singlet states A_{1g} and E_{1g} (Ref. 33) or the pair of odd states A_{1u} and E_{1u}.[34] This remarkable choice of the A_1 and E_1 order parameters irrespective of their parity results seemingly from some approximate symmetry of the crystal field. A phenomenological assumption about a weak crystal lattice effect on superconductivity in UPt_3 has been proposed in Ref. 10. The kink in the H-T plane at $P=0$ and the qualitative structure of the P-T phase diagram were explained assuming a nearly degenerate d-wave superconducting order parameter. UPt_3 shows, however, anisotropic properties in the normal state and a naive isotropic superconducting pairing is hardly expected. In addition, the controversy remains about even or odd parity of the pairing function in connection with an almost constant Knight shift below T_c (Ref. 35) and an unusual temperature dependence of the anisotropy of the upper critical field.[36,33]

We therefore formulate a different phenomenological model, which is a combination of the proposals of Refs. 6,10. Namely, we study the mixture of accidentally degenerate A_1 and E_1 order parameters, both even or odd, using the assumption that the crystal lattice does not affect significantly their interactions. Only under this assumption is a quantitative treatment of the AE model simple and most of results can be expressed in an analytical form. Our aim is to show that the whole H-T diagram of the superconducting states in UPt_3 at both $P<P_{\rm cr}$ and $P>P_{\rm cr}$ can be explained and fitted with experimental data in this simplified version of the AE model. We consider also the measurements by Lin *et al.*[17] of the magnetic phase diagram in a tilted field, which show features in the behavior of transition lines near the tetracritical point.

II. MODEL

We first assume that the electrons in UPt_3 form pairs with the total momentum $J=2$ in a nearly isotropic environment. In this model the lower symmetry of the crystal lattice causes only a slight splitting of the transition temperature of a fivefold degenerate multiplet of the Cooper pairs. Considerations of the singlet (d-wave) and the triplet (p-wave with strong spin-orbital coupling) order parameters are completely analogous. Therefore, for the the reader's convinience, we will use in the following basis functions corresponding to d-wave pairing:

$$\hat{\Delta}(\mathbf{k})=\sum_{i,j} B_{ij}k_ik_j=\tfrac{1}{2}a_{\pm 2}(k_x\pm ik_y)^2+a_{\pm 1}(k_x\pm ik_y)k_z + \frac{1}{\sqrt{6}}a_0(k_x^2+k_y^2-2k_z^2). \tag{1}$$

Our analysis starts from the corresponding SO(3)-invariant GL functional, which we write in terms of 3×3, symmetric, traceless matrix B:

$$F=\alpha(T-T_c)\mathrm{Tr}B^*B+\beta_1(\mathrm{Tr}B^*B)^2+\beta_2|\mathrm{Tr}B^2|^2 + \beta_3\mathrm{Tr}B^{*2}B^2+K_1D_i^*B_{jk}^*D_iB_{jk}+K_2D_i^*B_{ik}^*D_jB_{jk} + K_3D_i^*B_{jk}^*D_jB_{ik}+\frac{\mathbf{h}^2}{8\pi},\quad D_i=\partial_i-i\frac{2e}{\hbar c}A_i. \tag{2}$$

The weak-coupling approximation imposes the following relations on the phenomenological parameters: $\beta_2=0.5\beta_1$, $\beta_3=0$, $K_2=K_3=2K_1$. As was shown by Mermin,[37] who studied the functional (2) in connection with superfluid phases of ^{3}He, two different phases correspond to the ground state under the condition $\beta_2>0$:

$$\hat{\Delta}(\mathbf{k})\sim(k_x+ik_y)^2, \quad \beta_3>0, \tag{3}$$

$$\hat{\Delta}(\mathbf{k})\sim k_x^2+e^{2\pi i/3}k_y^2+e^{4\pi i/3}k_z^2, \quad \beta_3<0. \tag{4}$$

These solutions are unique up to multiplication by a phase factor and rotation of coordinate axes. The case $\beta_3=0$ is degenerate, and any matrix B satisfying $\mathrm{Tr}B^2=0$ would minimize the GL functional (2). The magnitude of β_3 is determined by strong-coupling effects $\beta_3\sim T_c/E_F$ and should be small even for UPt_3 with $E_F\approx 10$ K. This smallness of β_3 is important in our description of the observed P-T phase diagram.

The crystal field splits a single transition temperature T_c in accordance with irreducible representations of the D_6 point group:[38,39]

$$\begin{aligned} &A_1: k_x^2+k_y^2-2k_z^2, T_0, \\ &E_1: (k_x\pm ik_y)k_z, T_1, \\ &E_2: (k_x\pm ik_y)^2, T_2. \end{aligned} \tag{5}$$

The direction of $\hat{\mathbf{z}}$ is along the c axis. We suggest that the effect which primarily determines the structure of the phase diagram is the splitting of the transition temperature for the fivefold degenerate order parameter. We ignore the effect of the crystal lattice on the fourth-order and gradient terms in (2), because it can only slightly change the picture derived below.

Symmetry arguments place no restrictions on the order of critical temperatures (5), which may change under pressure.

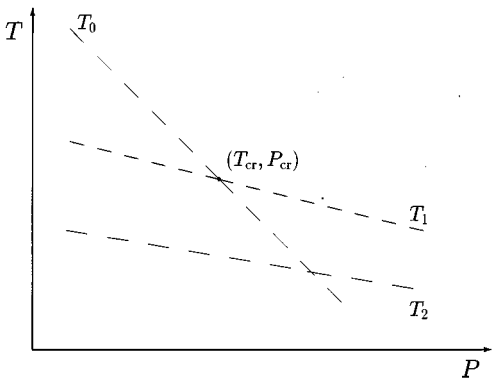

FIG. 1. Pressure dependence of critical temperatures for irreducible representations (5) assumed in the AE model.

Analysis of all possible cases reveals that the UPt_3 phase diagram can be explained with a single arrangement of critical temperatures in the P-T plane as shown in Fig. 1. Namely, the policritical point (P_{cr},T_{cr}) is determined by the intersection of lines $T_0(P)$ and $T_1(P)$, while the E_2 representation is not involved in the observed transitions. This conclusion of the phenomenological theory is in agreement with microscopic calculations.[33,34] Finally, the GL functional of our model is given by (2) with split T_c and excluded components of the E_2 representation. We will write explicitly homogeneous and gradient terms of this functional in the following sections.

III. ZERO-FIELD PHASE DIAGRAM

For investigation of superconducting phases in zero magnetic field we may restrict ourselves to homogeneous terms for the A_1 and E_1 representations, and rewrite the free energy density (2) in the form

$$\begin{aligned} F=&\alpha(T-T_0)|a_0|^2+\alpha(T-T_1)(|a_1|^2+|a_{-1}|^2)+\beta_1(|a_0|^2+|a_1|^2+|a_{-1}|^2)^2+\beta_2|a_0^2+2a_1a_{-1}|^2 \\ &+\beta_3[\tfrac{1}{2}|a_0|^4+\tfrac{1}{4}(|a_1|^4+|a_{-1}|^4)+\tfrac{3}{2}|a_1|^2|a_{-1}|^2+\tfrac{1}{6}|a_0|^2(|a_1|^2+|a_{-1}|^2)+\tfrac{5}{6}(a_0^{*2}a_1a_{-1}+\text{c.c.})]. \end{aligned} \tag{6}$$

This GL functional for a three-component order parameter is more complicated than functionals studied previously for UPt_3;[3,7,13] however, its analysis can be also done analytically. Let us first investigate superconducting phases which minimize (6), neglecting the last fourth-order term with small coefficient β_3. We consider the case $\beta_2>0$ only, which gives an adequate description for UPt_3 as we will see.

At pressures below P_{cr}, the upper transition takes place at $T_c^+=T_0$ to the phase

$$\hat{\Delta}_1(\mathbf{k})=\frac{a_0}{\sqrt{6}}(k_x^2+k_y^2-2k_z^2), \quad a_0^2=\frac{\alpha(T_0-T)}{2(\beta_1+\beta_2)},$$

$$F_1=-\frac{\alpha^2(T_0-T)^2}{4(\beta_1+\beta_2)}. \tag{7}$$

The energy gap of the phase $\hat{\Delta}_1(\mathbf{k})$ in the case of d-wave pairing has two lines of nodes whose position on the Fermi surface is determined by $\cos^2\theta=1/3$. The order parameter (7) does not minimize the second fourth-order term in (6). Therefore, the lower second-order phase transition occurs at $T=T_c^-$:

$$T_c^-=\frac{1}{2}\left[T_0\left(1-\frac{\beta_1}{\beta_2}\right)+T_1\left(1+\frac{\beta_1}{\beta_2}\right)\right]. \tag{8}$$

Below T_c^- the free energy achieves its minimum value for the complex order parameter with broken time-reversal symmetry:

$$\hat{\Delta}_2(\mathbf{k})=\frac{a_0}{\sqrt{6}}(k_x^2+k_y^2-2k_z^2)+irk_xk_z, r^2=\frac{\alpha(T_c^- -T)}{2\beta_1},$$

$$a_0^2=\frac{r^2}{2}+\frac{\alpha(T_0-T_1)}{4\beta_2},$$

$$F_2=-\frac{\alpha^2(T_0+T_1-2T)^2}{16\beta_1}-\frac{\alpha^2(T_0-T_1)^2}{16\beta_2}. \quad (9)$$

The rotational symmetry around the c axis is also broken for the phase $\hat{\Delta}_2(\mathbf{k})$, which is invariant under the residual symmetry group $D_2(U_{2y})$. After T_c^- the lines of zeros in the energy gap are smeared, leaving only four-point nodes.

The ratio of the heat capacity jumps at the upper and lower transitions is

$$\frac{(\Delta C/T)|_{T_c^-}}{(\Delta C/T)|_{T_c^+}}=\frac{\beta_2}{\beta_1}. \quad (10)$$

Note that Eqs. (8) and (10) are exactly the same as for the SBF or AB models.

At pressures above $P_{\rm cr}$, the superconducting transition takes place at $T_c=T_1$ to the phase

$$\hat{\Delta}_3(\mathbf{k})=a_1(k_x+ik_y)k_z, \quad a_1^2=\frac{\alpha(T_1-T)}{2\beta_1},$$

$$F_3=-\frac{\alpha^2(T_1-T)^2}{4\beta_1}. \quad (11)$$

Its symmetry group is $D_6(E)$. The state $\hat{\Delta}_3(\mathbf{k})$ corresponds to the minimum of the fourth-order term multiplied by β_2. Therefore, the transition with an admixture of the a_0 component is completely suppressed at $P>P_{\rm cr}$. On the phase diagram in the P-T plane there will be a temperature-independent fourth line of transitions between $\hat{\Delta}_2(\mathbf{k})$ and $\hat{\Delta}_3(\mathbf{k})$ states. This transition is of first order as $D_2(U_2)\not\subset D_6(E)$. The jump in the volume on this line is

$$\frac{\Delta V}{V}=\frac{\alpha^2(T_{\rm cr}-T)}{4\beta_1}\left(\frac{\partial T_1}{\partial P}-\frac{\partial T_0}{\partial P}\right). \quad (12)$$

Let us consider now the effect of nonzero β_3. Obviously, the symmetries of all phases remain the same. The change at $P<P_{\rm cr}$ is only quantitative and consists of the substitution

$$\beta_1\to(\beta_1+\tfrac{1}{12}\beta_3), \quad \beta_2\to(\beta_2+\tfrac{5}{12}\beta_3) \quad (13)$$

in all formulas (7)–(10). The energy of the state $\hat{\Delta}_3(\mathbf{k})$ is obtained from (11) by the replacement $\beta_1\to(\beta_1+\frac{1}{4}\beta_3)$. The phase (11) does not minimize the third fourth-order term in (6) for $\beta_3>0$. As a result, the fourth transition line in the P-T diagram deviates from the vertical position. Equating the energies of the phases (9) and (11) we obtain in first order in a small parameter β_3/β_1 the second transition temperature

$$T^*(P)=T_1(P)-\frac{6\beta_1}{\beta_3}[T_1(P)-T_0(P)]. \quad (14)$$

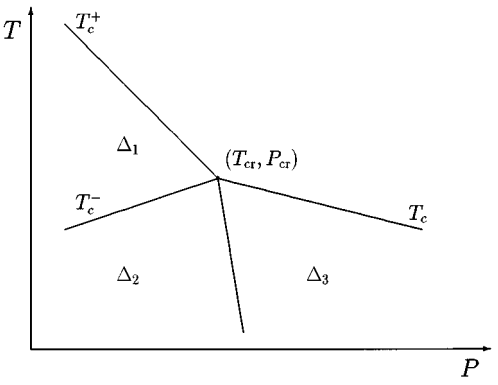

FIG. 2. Schematic zero-field diagram of UPt_3.

The resulting phase diagram is shown in Fig. 2. Due to the small slope with respect to the T axis, the effective width of the transition on this fourth boundary observed in the temperature sweep experiments significantly increases, which made earlier attempts at detection of the $T^*(P)$ line unsuccessful.

Boukhny *et al.*[16] found the trace of the fourth phase boundary in the P-T plane by the study of the H-T diagram at uniaxial pressures above $P_{\rm cr}$. Applying Eq. (14) to their results we obtain the estimation $\beta_3\sim 0.1$–$0.2\beta_1$. As β_3 is multiplied small factors in the corresponding formulas (13), we will disregard below its influence on the thermodynamic properties.

A few remarks are needed concerning our neglect of the E_{2g} representation, which may have a nonzero critical temperature $T_2<T_0, T_1$. The symmetry of the phase $\hat{\Delta}_2(\mathbf{k})$ allows an admixture of $a_2=a_{-2}$ with a real phase. As the mixing term is proportional to β_3, the components a_2 and a_{-2} have smallness of the order of β_3/β_1 compared to a_0 and $a_1=a_{-1}$. Then, the correction to the free energy is of the order of $(\beta_3/\beta_1)^2$ and may be neglected. The positive β_3 can also stabilize at low temperatures the phase with another symmetry (3), as is the case for the degenerate T_c.[37] However, comparison of the energy of this phase with the energy (11) gives the result that such a transition between phases (3) and (11) will not occur until 0 K if $(T_1-T_2)/T_1>\beta_3/(8\beta_1)$. Even a weaker condition is required for the stability of the phase $\hat{\Delta}_2(\mathbf{k})$; hence our analysis yields true low-temperature phases for a wide range of the values of T_2.

IV. UPPER CRITICAL FIELD

In this section we investigate the superconducting transition in a magnetic field for different orientations of **H** with respect to crystal axes and for $P<P_{\rm cr}$. The upper critical field is anisotropic due to the splitting of critical temperature by crystal field in the SO(3)-invariant energy functional (2). To determine $H_{c2}(T)$ we solve the linearized GL equations derived from (2), omitting the E_2 components and assuming a uniform order parameter along the field. The corresponding solutions and their critical fields depend on phenomenologi-

cal parameters K_i in gradient terms. The parameter K_1 is inversely proportional to the effective electron mass and scales critical fields for all superconducting phases. We also assume $K_2=K_3$, because their difference is relatively small: $(K_2-K_3)\sim(T_c/E_F)^2$,[40] and define a dimensionless phenomenological parameter $C=K_2/K_1=K_3/K_1$. The parameter C determines the form of the H-T phase diagram in our model. (In the weak-coupling approximation $C=2$.)

A. Magnetic field along the *c* axis

In this case the gradient energy for the A_1 and E_1 representations is

$$F_{\rm grad}=K_1\left[\left(1+\frac{C}{3}\right)|D_i a_0|^2+\left(1+\frac{C}{2}\right)|D_i a_{\pm1}|^2 + \frac{C}{2}(D_-^* a_{-1}^* D_+ a_1+D_+^* a_1^* D_- a_{-1})\right], \quad (15)$$

where $i=x,y$ and $D_\pm=D_x\pm iD_y$. Linearized GL equations separate for (15) into a system of two coupled equations on amplitudes a_1 and a_{-1} and an independent equation on a_0. As in the ordinary case these equations can be solved by defining the lowering and raising operators

$$\hat a=\left(\frac{\hbar c}{4|e|H}\right)^{1/2}(D_x-iD_y),\quad [\hat a,\hat a^+]=1, \quad (16)$$

and expanding each component of the order parameter in a series of Landau level functions $f_n(\mathbf{r})$, $\mathbf{r}$ denotes position of the center of mass of the pair. The solution for the component a_0 with the lowest eigenvalue and the highest critical field has the usual form

$$\hat\Delta^{(0)}(\mathbf{k},\mathbf{r})=\frac{f_0(\mathbf{r})}{\sqrt6}(k_x^2+k_y^2-2k_z^2),$$

$$\lambda_0=1+\frac{C}{3},\quad H^{(0)}(T)=\frac{\Phi_0}{2\pi}\frac{\alpha(T_0-T)}{K_1\lambda_0}, \quad (17)$$

with Φ_0 being the flux quantum. On the other hand, the system of two coupled equations is satisfied by a more complicated eigenstate[41]

$$\hat\Delta^{(1)}(\mathbf{k},\mathbf{r})=f_0(\mathbf{r})(k_x+ik_y)k_z+\omega f_2(\mathbf{r})(k_x-ik_y)k_z,$$

$$\lambda_1=3\left(1+\frac{C}{2}\right)-\sqrt{2C^2+(2+C)^2},$$

$$\omega=-\frac{\sqrt2 C}{5\left(1+\frac{C}{2}\right)-\lambda_1},\quad H^{(1)}(T)=\frac{\Phi_0}{2\pi}\frac{\alpha(T_1-T)}{K_1\lambda_1}. \quad (18)$$

The nonfactorized dependence of $\hat\Delta^{(1)}(\mathbf{k},\mathbf{r})$ on $\mathbf{k}$ and $\mathbf{r}$ is a consequence of the classification of eigenstates of the order parameter at H_{c2} by the generalized Landau level number $N=n+m$, where m is the projection of the internal angular momentum of the pair on the field direction.[42] For the phases (17) and (18), $N=0$ and $+1$, respectively.

In a wide range of values of C we have $\lambda_0>\lambda_1$ and, consequently, the slope of the $H^{(1)}(T)$ curve is larger than that of $H^{(0)}(T)$. As they start from different temperatures and $T_0>T_1$ at $P=0$, a kink should appear in the temperature dependence of the upper critical field $H_{c2}=\max\{H^{(0)}(T),H^{(1)}(T)\}$. Such a kink in $H_{c2}(T)$ for $\mathbf{H}\|c$ was not detected in early experiments on the phase diagram of UPt_3, reflecting a small difference between λ_0 and λ_1. However, it was confirmed later by the existence of a well-defined tetracritical point for this orientation of the field which is formed by an *intersection* of two different lines of transitions in the H-T plane.[1] This tetracritical point is situated relatively far from T_c, in the region where nonlinear corrections to the GL approximation become significant. Therefore, we will fit the experimental curve $H_{c2}(T)$ in UPt_3 and find the phenomenological parameter C by data for the another field orientation $\mathbf{H}\perp c$.

B. Magnetic field in the basal plane

The GL functional (2) with split T_c possesses rotational symmetry about the c axis. Therefore, the upper critical field is isotropic in the basal plane. We assume $\mathbf{H}\|\hat{\mathbf{x}}$. It is convenient to define complex amplitudes instead of a_1 and a_{-1},

$$a_{\pm1}=\frac{\eta_x\mp i\eta_y}{\sqrt2}, \quad (19)$$

which coincide with the usual expansion coefficients for the E_1 representation.[38,39] In our notation the quadratic part of the energy (2) is

$$F=\alpha(T-T_0)|a_0|^2+\alpha(T-T_1)(|\eta_x|^2+|\eta_y|^2)+K_1\left[\left(1+\frac{C}{3}\right)|D_y a_0|^2+\left(1+\frac{4}{3}C\right)|D_z a_0|^2+|D_y\eta_x|^2 + (1+C)(|D_z\eta_x|^2+|D_y\eta_y|^2+|D_z\eta_y|^2)-\frac{C}{2\sqrt3}(D_y^*\eta_y^* D_z a_0+D_z^*\eta_y^* D_y a_0+\text{c.c.})\right]. \quad (20)$$

The corresponding linearized GL equations separate again into a system for the a_0 and η_y components and an independent equation for η_x. Because of the uniaxial symmetry, gradients along $\hat{\mathbf{y}}$ and $\hat{\mathbf{z}}$ directions enter (20) with different factors. As is known from the theory of anisotropic conventional superconductors,[43] the expression $K_yD_y^2+K_zD_z^2$ can be written in an isotropic form $\sqrt{K_yK_z}(D_{y'}^2+D_{z'}^2)$ by applying the scaling transformation

$$y'=sy, \quad z'=z/s, \quad s=(K_z/K_y)^{1/4}. \tag{21}$$

With the help of this transformation one can find the following eigenstate:

$$\hat{\Delta}^{(1)}(\mathbf{k},\mathbf{r})=f_0(\mathbf{r}')\sqrt{2}k_xk_z, \quad \lambda_1=\sqrt{1+C}, \quad s_1=(1+C)^{1/4},$$

$$H^{(1)}(T)=\frac{\Phi_0}{2\pi}\frac{\alpha(T_1-T)}{K_1\lambda_1}. \tag{22}$$

The diagonal terms for the a_0 and η_y components, however, cannot be written in isotropic form simultaneously, which leads to the problem of finding the lowest eigenvalue in an infinite-dimension system. We solve this problem numerically, developing a perturbation theory for the coupling term. Calculations are described in more detail in the next subsection. Here we only formulate the result: For $T_1<T_0$ it is possible to neglect the admixture of η_y and to obtain the second solution analytically:

$$\hat{\Delta}^{(0)}(\mathbf{k},\mathbf{r})=\frac{f_0(\mathbf{r}')}{\sqrt{6}}(k_x^2+k_y^2-2k_z^2),$$

$$\lambda_0=\sqrt{(1+C/3)(1+4C/3)}, \quad s_0=\left(\frac{1+4C/3}{1+C/3}\right)^{1/4},$$

$$H^{(0)}(T)=\frac{\Phi_0}{2\pi}\frac{\alpha(T_0-T)}{K_1\lambda_0}. \tag{23}$$

Because of the difference in slopes ($\lambda_0>\lambda_1$, for $C>0$), the curves $H^{(0)}(T)$ and $H^{(1)}(T)$ intersect at the point

$$T_k=\frac{T_1\lambda_0-T_0\lambda_1}{\lambda_0-\lambda_1}, \quad H_k=\frac{\Phi_0}{2\pi}\frac{\alpha(T_0-T_1)}{K_1(\lambda_0-\lambda_1)}, \tag{24}$$

producing a kink in the temperature dependence of the upper critical field. The quantum number different for the two eigenstates (22) and (23) is the parity of the order parameter under reflections in the plane perpendicular to **H**.

C. Arbitrary directed magnetic field

Assuming magnetic field in the x-z plane, $\mathbf{H}=(H\sin\theta,0,H\cos\theta)$, we choose a coordinate frame with the $\tilde{z}$ axis parallel to **H** and the $\tilde{y}$ axis parallel to $\hat{\mathbf{y}}$. If we omit gradients along $\tilde{z}$, and drop the tilde over our coordinates, the gradient energy can be written as

$$F_{\rm grad}=K_1\left[\left(1+\frac{C}{3}+C\sin^2\theta\right)|D_xa_0|^2+\left(1+\frac{C}{3}\right)|D_ya_0|^2+(1+C)(|D_x\eta_x|^2+|D_y\eta_y|^2)+|D_y\eta_x|^2+(1+C\sin^2\theta)|D_x\eta_y|^2\right.$$
$$+\frac{C}{2\sqrt{3}}\sin\theta(D_x^*a_0^*D_y\eta_y+D_y^*a_0^*D_x\eta_y+\text{c.c.})+\frac{C}{2\sqrt{3}}\sin2\theta(D_x^*a_0^*D_x\eta_x+\text{c.c.})+\frac{C}{2}\cos\theta(D_x^*\eta_x^*D_y\eta_y$$
$$\left.+D_y^*\eta_x^*D_x\eta_y+\text{c.c.})\right]. \tag{25}$$

For a general direction of the field ($\theta\neq0,\pi/2$) there are no quantum numbers which may be ascribed to different eigenstates of the linear problem. Therefore, an intersection of levels is prohibited and $H_{c2}(T)$ is a smooth curve.

To find a smearing of kink in a tilted magnetic field the differential linearized GL equations derived from (25) have to be solved. We calculate the corresponding upper critical field numerically using the following perturbation scheme. Turning off all three coupling terms in (25) we get three independent equations on a_0, η_x, η_y. Solutions of this zeroth-order approximation are known. They are sets of Landau level functions obtained for each component by its own scaling transformation: $y'=s_ky$, $x'=s_k^{-1}x$, with $k=0,x,y$. We expand the components a_0, η_x, η_y in terms of these three complete sets of basis functions and transform the differential equations to an infinite-dimension algebraic system. The off-diagonal terms in this system are given by the matrix elements of coupling terms between eigenstates of different components. They can be easily calculated choosing a particular gauge, e.g., $\mathbf{A}=(-Hy,0,0)$. The eigenvalues of the linearized GL equations are obtained, then, by a truncation of the infinite matrix.

The first-order iteration is to omit all eigenstates except the zeroth Landau level functions and, then, to diagonalize the resulting system of three equations numerically. At the second step we allow the admixture of the second Landau level functions and diagonalize a system of six equations and so on. (Odd-number Landau levels are not admixed due to the remaining conserved quantum number, which is the parity of N.[42]) We do not write explicitly the cumbersome expressions for the matrix elements, but present, instead, results of the first two iterations for $T_0=1$, $T_1=0.9$, $C=2$, and $\theta=45°$ in Fig. 3. It can be seen that the proposed iteration procedure converges very rapidly, and an accuracy better than 1% can be already achieved by diagonalizing the 6×6 matrix.

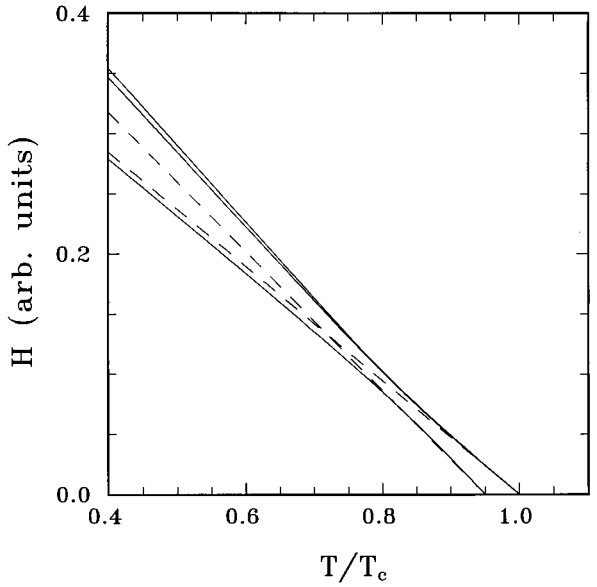

FIG. 3. Subsequent iterations for critical fields of different eigenstates in the *AE* model with magnetic field at 45° to the *c* axis and parameters from the text. Dashed lines correspond to the zeroth-order approximation.

D. Comparison with experiment

We now compare the results of this section with experimental data. We choose for this purpose ultrasonic velocity measurements[17,44] which give the *H-T* phase diagram of UPt_3 at zero pressure for three orientations of field $\theta = 0°$, 45°, and 90°. As the experimental $H_{c2}(T)$ curve for $\mathbf{H} \| c$ shows a significant curvature, we fit first the upper critical field for $\mathbf{H} \perp c$ (Ref. 44) under the assumption that all transition lines are perfectly straight. Parameters derived from the experimental values of the critical temperatures $T_0 = T_c^+ = 499$ mK, $T_1 = 476$ mK, $T_k = 403$ mK with the help of Eq. (24) are

$$\lambda_0/\lambda_1 = 1.31, \quad C = 1.34, \tag{26}$$

while K_1 is chosen so as to agree with observed values of the critical fields [Fig. 4(a)].

The upper critical field for $\mathbf{H} \| c$ calculated for the same set of parameters is presented in Fig. 4(b). Though the approximation of the $H_{c2}(T)$ curve by straight lines predicts the intersection (kink) point at a higher temperature, the actual difference is not very large. Moreover, our formulas reproduce well the observed anisotropy of the upper critical field in the vicinity of T_c.

A common argument against the *AE* model is that it predicts a smearing of the kink for intermediate directions of the magnetic field. We plot an experimental diagram for $\theta = 45°$ (Ref. 17) together with our numerically calculated $H_{c2}(T)$ curve in Fig. 5. As the sample used in 45° measurements is different from that used in Ref. 44, we choose new values of the critical temperature $T_c^+ = T_0$ and of the coherence length (K_1) in our calculations. However, the relative differences between the critical temperatures of the two representations $(T_0 - T_1)/T_0 = 0.954$ and the parameter C are kept the same.

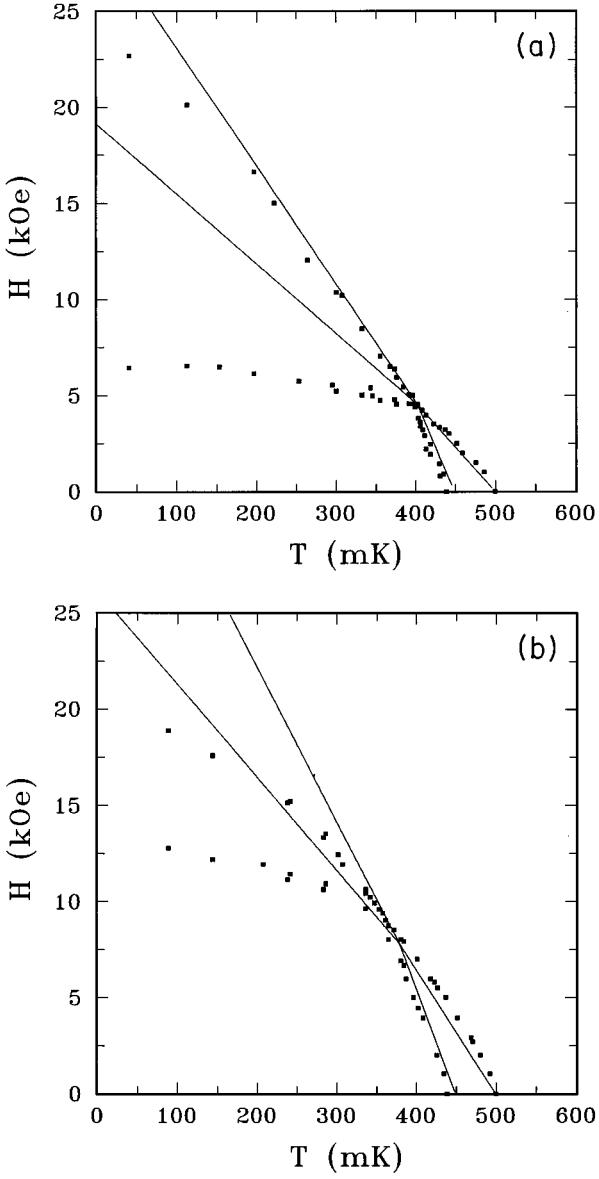

FIG. 4. Calculated phase boundaries (solid lines) and experimental data derived from ultrasonic velocity measurements (Ref. 46) for two directions of the magnetic field (a) $\mathbf{H} \perp c$ and (b) $\mathbf{H} \| c$.

Contrary to the statement in Ref. 17 about the clearly observed kink in the temperature dependence of the upper critical field, one can see that the experimental data are reasonably fitted by a smooth curve. A feature of the experimental phase diagram for the field directed at 45° to the *c* axis is an ''intersection'' of the inner transition lines apart from the $H_{c2}(T)$ curve. This feature was interpreted as the existence of two critical points instead of the single tetracritical point in the *H-T* plane.[17] Note that this is not allowed thermodynamically, if all lines correspond to the second-order phase transitions.[25] We can not exclude *a priori* the possibility to construct a model for such a splitting of the tetracritical point into two points connected by a line of first-order transitions for intermediate directions of the field; however, its origin is completely unclear in the framework of theories presented so far.[2–15] A more natural interpretation of this behavior of the inner lines is a smearing of the kink point with the repulsion

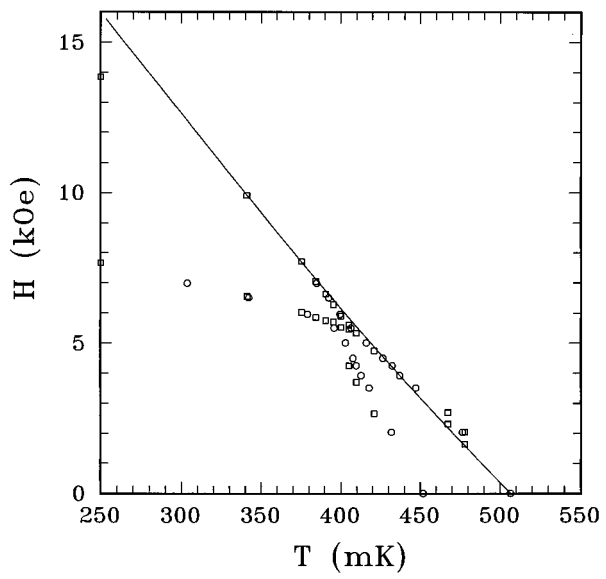

FIG. 5. Experimental phase diagram (Ref. 17) and the upper critical field calculated in the *AE* model (solid line) for the magnetic field directed at 45° with respect to the *c* axis.

of two nonintersecting levels of the linear problem, as is expected for the *AE* model. The analogous smearing of the kink exists also in the E_{1g} model,[15] but it is expected to be more significant for $\mathbf{H}\|c$ than for $\mathbf{H}$ at 45° to the *c* axis, which is not confirmed by the experiment.[17,44]

V. PHASE TRANSITIONS INSIDE A MIXED STATE

Structural phase transitions in the flux lattice are, perhaps, the most striking feature in a macroscopic behavior of a multicomponent superconductor. The vortex states near the lower critical field H_{c1} were studied for the two-component E_1 order parameter using the numerical relaxation techniques in Refs. 26–28. Hirano *et al.*[12] presented numerical results obtained by the same method for intermediate fields and fields close to H_{c2}. However, examination of vortex lattices in the vicinity of the upper critical field admits a significant simplification due to the fact that the spatial form of the order parameter is determined by the linearized GL equations. Phase transitions inside the mixed state have been studied in this approximation by a number of authors[29,30,8] (see also Ref. 42 for a review). We calculate using the same analytical approach, which is undoubtedly true near the tetracritical point in the *H-T* diagram of UPt_3, the inner phase boundaries between different vortex states in our model.

The general procedure is to expand the superconducting order parameter into the two eigenstates under consideration [either (17) and (18) or (22) and (23)],

$$\hat{\Delta}=\mu_0\hat{\Delta}^{(0)}+\mu_1 e^{i\phi}\hat{\Delta}^{(1)}, \tag{27}$$

and substitute this ansatz into the GL functional.

Working in the limit of large values of the GL parameter κ_{GL}, we can neglect the contribution of superconducting currents and write the free energy density near the upper critical field in the universal form

$$F=\alpha'\lambda_0(H-H_0)\mu_0^2+\alpha'\lambda_1(H-H_1)\mu_1^2+\delta_0\mu_0^4+\delta_1\mu_1^4 +2\delta_{\mathrm{int}}\mu_0^2\mu_1^2, \tag{28}$$

where $\alpha'=2\pi K_1/\Phi_0$. The energetic parameters δ_0 and δ_1 are analogs of Abrikosov's parameter for conventional superconductors,[45] while δ_{int} represents the interaction between $\hat{\Delta}^{(0)}$ and $\hat{\Delta}^{(1)}$. These parameters depend on the particular form of the eigenstates and on the fourth-order terms. We write them explicitly for $\mathbf{H}\|c$ and $\mathbf{H}\perp c$ below. But before that let us consider general conclusions which can be derived from the universal two-order parameter functional (28).

By minimization of (28) with respect to the expansion coefficients μ_0 and μ_1, the following sequence of superconducting states is found for $H_0>H_1$. In close vicinity of the upper critical field $H_{c2}=H_0$ only one eigenstate appears with the energy

$$F_0=-\alpha'^2\lambda_0^2\frac{(H_0-H)^2}{4\delta_0}. \tag{29}$$

An infinite degeneracy of the order parameter is lifted by nonlinear interactions and the form of the vortex lattice may be determined by substitution of an arbitrary periodic solution for $\hat{\Delta}^{(0)}$ in the energy parameter δ_0 and its subsequent minimization.

The vortex lattice for the $\hat{\Delta}^{(0)}$ component becomes unstable towards an admixture of the second eigenstate $\hat{\Delta}^{(1)}$ at

$$H_{FL}=H_1-\frac{H_0-H_1}{\lambda_1\delta_0/\lambda_0\delta_{\mathrm{int}}-1}. \tag{30}$$

Below this field the superconducting phase consists of two interpenetrating vortex lattices formed by each eigenstate. On the phase transition line the periodic structure of $\hat{\Delta}^{(1)}$ should coincide with the form found previously for $\hat{\Delta}^{(0)}$, while minimization of δ_{int} (in order to achieve the highest H_{FL}) gives the displacement between two sublattices as well as their relative phase ϕ. After the phase transition the free energy density is given by

$$F=F_0-\alpha'^2\frac{(\lambda_1\delta_0-\lambda_0\delta_{\mathrm{int}})^2}{\delta_0\delta_1-\delta_{\mathrm{int}}^2}\frac{(H_{FL}-H)^2}{4\delta_0}. \tag{31}$$

For the other relation between critical fields, $H_1>H_0$, all formulas may be obtained directly from Eqs. (29)–(31) by interchange of the indices $0\leftrightarrow 1$.

A. Magnetic field along the *c* axis

The energetic parameters defined above are given for the phases (17) and (18) by

$$\delta_0=(\beta_1+\beta_2)\frac{\langle|\tilde{f}_0|^4\rangle}{\langle|\tilde{f}_0|^2\rangle^2}, \tag{32}$$

$$\delta_1=\frac{\beta_1\langle|f_0|^4+\omega^4|f_2|^4\rangle+2(\beta_1+2\beta_2)\omega^2\langle|f_0|^2|f_2|^2\rangle}{(1+\omega^2)^2\langle|f_0|^2\rangle^2}, \tag{33}$$

$$\delta_{\rm int}=\frac{\beta_1\langle|\tilde f_0|^2|f_0|^2+\omega^2|\tilde f_0|^2|f_2|^2\rangle+\beta_2\omega\langle\tilde f_0^{*2}f_0f_2+\text{c.c.}\rangle}{(1+\omega^2)\langle|f_0|^2\rangle\langle|\tilde f_0|^2\rangle}. \tag{34}$$

A tilde serves to distinguish zeroth Landau level functions for different eigenstates and brackets denote the spatial average. The general expression for one-quantum periodic solutions $f_n(\mathbf{r})$ invariant under elementary translations on $\mathbf{a}=(a,0)$ and $\mathbf{b}=(b\cos\alpha,b\sin\alpha)$ is

$$f_n(\mathbf{r})\sim\sum_m \exp\left[-\pi i\rho m^2+\frac{2\pi}{a}imx-\frac{1}{2}(y-mb\sin\alpha)^2\right]H_n(y-mb\sin\alpha), \tag{35}$$

where $H_n(y)$ is the Hermitian polynomial of the nth order and all distances are measured in the units of magnetic length $l_H^2=\hbar c/2|e|H$. The form of the vortex lattice is determined by two parameters $\rho=b/a\cos\alpha$ and $\sigma=b/a\sin\alpha$, while the area of the unit cell is fixed by the flux quantization rule $ab\sin\alpha=2\pi$. The dependence of energetic parameters on ρ and σ may be found by substitution of (35) in (32)–(34) and integration over x and y.[45,42]

For the phase (17) the energetic parameter δ_0 is identical to what appears in the theory of conventional superconductors.[45] Its minimum value $\delta_0=1.160(\beta_1+\beta_2)$ is achieved for the one-quantum perfect triangular lattice with $\rho=\frac{1}{2}$ and $\sigma=\sqrt{3}/2$. The energetic parameter δ_1 for the phase (18) is more complicated as a consequence of the admixture of two components a_1 and a_{-1} simultaneously.[42] The possible types of vortex structure for this phase include perfect triangular, square, rectangular, and other lattices. However, if the phenomenological parameters β_2 and C are not far from their weak-coupling values, the stable form is again the perfect triangular lattice. Having the same form, vortex lattices for the eigenstates $\hat\Delta^{(0)}$ and $\hat\Delta^{(1)}$ differ in the phase factors gained under rotations on 60° and in the parity under reflections in the basal plane.[42]

We next investigate the vortex structure of the combined solution. The vortex lattice $\tilde f_0(\mathbf{r})$ displaced from (35) by $\mathbf{r}_0=(x_0,y_0)$ can be obtained substituting $(x-x_0)$ and $(y-y_0)$ instead of x and y and applying simultaneously the gauge transformation $\exp(iy_0x)$. We will measure x_0 and y_0 in units of $(b\cos\alpha)$ and $(b\sin\alpha)$, respectively. The expression for the dependence of $\delta_{\rm int}$ on the displacement $\mathbf{r}_0$ is presented in the Appendix. For the two perfect triangular lattices there are three symmetrical relative positions shown in Fig. 6. In the first structure in Fig. 6(a), vortices of two sublattices coincide with each other; in the second structure in Fig. 6(b), vortices of the second sublattice appear at the centers of triangle sides of the background lattice, $x_0=1$, $y_0=0$; and in the third structure in Fig. 6(c), vortices of the second sublattice are located at the centers of triangles formed by vortices of the first sublattice, $x_0=1$, $y_0=\frac{1}{3}$.

The characteristic feature of the vortex structure with two displaced sublattices (27) is the breaking of translational invariance.[30,42] For example, the relative phase ϕ between $\hat\Delta^{(0)}$ and $\hat\Delta^{(1)}$ for the state in Fig. 6(b) changes by π under translation on $\mathbf{b}$. Thus, the vortex structure in Fig. 6(b) corresponds to a two-quantum lattice. The unit cell of the vortex lattice in Fig. 6(c) contains three quanta of the magnetic flux. Similar to antiferromagnets, the two-quantum vortex structure is still invariant under the combined transformation $\hat T_{\mathbf{b}}RU_{2y}$, where U_{2y} is rotation by π around the y axis. As the operation RU_{2y} does not change the magnetic field, this period multiplication cannot be observed in neutron diffraction experiments (see the next subsection).

Breaking of the translational symmetry is important in order to understand the role of the last phase-locking term

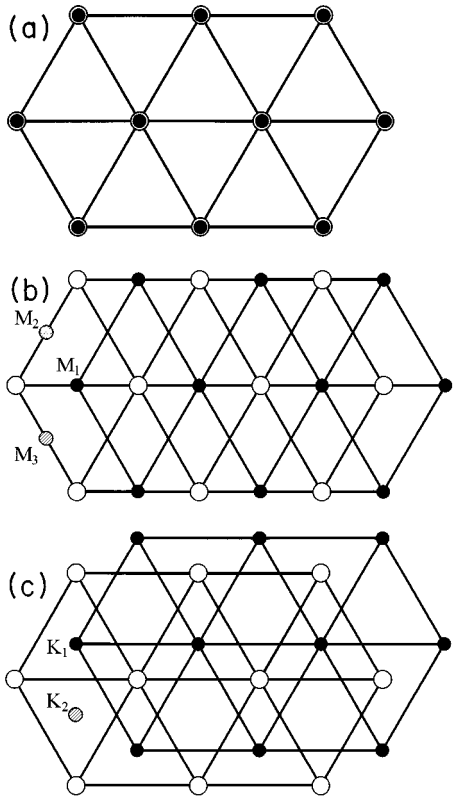

FIG. 6. Three most symmetric locations of the second vortex sublattice (solid circles) appearing below $H_{FL}(T)$ on the background of the first vortex sublattice (open circles): (a) undisplaced structure, (b) displacement on a half of a basis vector, and (c) displacement to the center of triangle. Dashed circles correspond to the equivalent positions for vortices of the second sublattice.

$(\hat{\Delta}^{(0)2}\hat{\Delta}^{(1)*2}+\text{c.c.})$ in δ_{int}. The phase-locking term is nonzero, if the relative phase ϕ changes 0 or π under translations, that is, only for the vortex structures in Figs. 6(a) and 6(b).[42] For the particular form of the interaction (34), rotational invariance makes the phase-locking term equal to zero for the coinciding structure [Fig. 6(a)] too. As a result, the two-quantum structure with a relative displacement between sublattices on a half lattice basis vector has a minimal energy for nonzero β_2 in the AE model. The phase transition at H_{FL} is accompanied by time-reversal symmetry breaking, i.e., $\phi=\pi/2$.

The phase-locking term for $\mathbf{H}\|c$ exists also in the AB model, and, as a consequence, the two-quantum vortex lattice has been found to be energetically favorable below H_{FL} in a wide range of parameters, including those derived from the experiment.[30,8] This prediction for the accidental degeneracy models is different from what is expected in the SBF models with a two-component order parameter. The phase-locking term is absent for $\mathbf{H}\|c$ in this case, and the three-quantum structure is stabilized.[30,42] [The opposite conclusion in Ref. 12 is a result of excluding the vortex configuration in Fig. 6(c) from their numerical analysis.]

Evidently, the rotational symmetry of the perfect triangular lattice is broken in the two-quantum structure. Hence, a continuous distortion of the lattice should appear below H_{FL}, which can result even in the stabilization of the square lattice. The threefold rotational symmetry is preserved in the vortex structure in Fig. 6(c) and the distortion of the lattice does not appear below the structural phase transition at H_{FL} in this case. Therefore, the observation of vortex lattices other than the perfect triangular one for $\mathbf{H}\|c$ would be important in order to distinguish between the accidental degeneracy models and the SBF scenarios[11,12] of the splitting in UPt_3, because the two groups of models have different vortex structures below H_{FL}.

B. Magnetic field in the basal plane

Vortex lattices and phase transitions in our model for this geometry are completely analogous to those in the SBF and AB models.[29,30,8] The spatial dependences of both components $a_0(\mathbf{r})$ and $\eta_x(\mathbf{r})$ are given by the scaled zeroth Landau level functions (22) and (23). Assuming $\mathbf{H}\|\hat{\mathbf{x}}$, we construct the following solution periodic along the y axis:

$$f_0(\mathbf{r}')\sim\sum_m \exp\left[-\pi i\rho m^2+\frac{2\pi}{a}imy-\frac{1}{2s^2}(z-mb\sin\alpha)^2\right]. \tag{36}$$

The distortion parameter s is equal to s_0 for the a_0 component and to s_1 for the η_x component. The energetic parameters, which determine the form of the vortex lattice and phase transition, are

$$\delta_0=(\beta_1+\beta_2)\frac{\langle|a_0|^4\rangle}{\langle|a_0|^2\rangle^2}, \tag{37}$$

$$\delta_1=(\beta_1+\beta_2)\frac{\langle|\eta_x|^4\rangle}{\langle|\eta_x|^2\rangle^2}, \tag{38}$$

$$\delta_{\text{int}}=\frac{\beta_1\langle|a_0|^2|\eta_x|^2\rangle+\frac{1}{2}\beta_2\langle a_0^{*2}\eta_x^2+\text{c.c.}\rangle}{\langle|a_0|^2\rangle\langle|\eta_x|^2\rangle}. \tag{39}$$

Being expressed in scaled coordinates (y',z'), the energy of solution (36) in the GL approximation coincides with that in the isotropic case and is independent of the orientation of vortex lattice in the y-z plane. This is in contrast with the residual twofold rotational symmetry of the system. The lower symmetry should result in the stabilization of one from the two most symmetric orientations of the lattice with the smallest side of the triangle either along the y or z axis. These two configurations are obtained from (36) by substitution of the lattice parameters $\rho=\frac{1}{2}$, $\sigma=(\sqrt{3}/2)s^2$ and $\rho=\frac{1}{2}$, $\sigma=(1/2\sqrt{3})s^2$, respectively. In conventional anisotropic superconductors the particular lattice orientation is determined by the nonlocal next-order terms in GL functional or by a small misorientation of the field. Besides that, in multicomponent superconductors, the above degeneracy is lifted at fields $H<H_{FL}$ by the admixture of the second component.[8]

It is convenient to investigate the phase transition at $H=H_{FL}$ in scaled coordinates corresponding to the eigenstate, which has the highest critical field. Then, this solution is given by (36) with $s=1$, while the second component is described by (36) with $s=s_1/s_0$ for $H_0>H_1$ or with $s=s_0/s_1$ for $H_1>H_0$. The phase-locking term in δ_{int} (39) plays again an important role in the choice between various displacements of two sublattices. The explicit expression for δ_{int} can be found in Ref. 8. This term is nonzero either for the undisplaced lattices [Fig. 6(a)] or for the two-quantum structure [Fig. 6(b)].

In contrast to the isotropic case discussed above, the center of the triangle is not a special symmetric point. Therefore, the structure in Fig. 6(c) is not extremal and vortices of the second sublattice are displaced above and below the point K, depending on the relation $s>1$ or $s<1$. The lower symmetry lifts also the degeneracy between different displacements on a half of a lattice basis vector. Namely, the energy of the two-quantum M_1 structure is different from the energy of the M_2 and M_3 structures. They depend also on the orientation of the first lattice, i.e., on the value $\sigma=\sqrt{3}/2$ or $\sigma=1/2\sqrt{3}$. Numerical evaluation of δ_{int} with parameters C and β_2 derived from the experiment (see next subsection) gives stability of the M_2 (M_3) structure with $\sigma=\sqrt{3}/2$ for $s>1$ and with $\sigma=1/2\sqrt{3}$ for $s<1$. The same structures have been found in the AB and SBF models.[8,12]

Straightforward generalization of the diamagnetic contribution near H_{c2} in conventional superconductors[45] yields the following expression for the magnetic field generated by superconducting currents in our case:

$$h_s=-\frac{8\pi|e|K_1}{\hbar c}(\lambda_0|a_0|^2+\lambda_1|\eta_x|^2). \tag{40}$$

This formula shows that though the gap function of the vortex structure for two displaced sublattices is not invariant under all elementary translations, the distribution of the magnetic field preserves periodicity with one quantum of the flux per unit cell. As we have mentioned above, for the M struc-

TABLE I. Parameters deduced from different measurements of the H-T diagram of UPt_3 for a magnetic field oriented in the basal plane.

Parameter	Ref. 46	Ref. 48	Ref. 49
C	1.34	1.27	1.45
β_2/β_1	0.233	0.290	0.254

ture this is due to the existence of combined invariance under the transformation $\hat{T}_{\mathbf{b}}RU_2$. The same conclusion holds for $\mathbf{H}\|c$ as well. Therefore, it is the one-quantum flux lattices which should be observed in the neutron diffraction measurements in UPt_3.[22] The period multiplication in the vortex lattice can be found only by phase sensitive techniques.

In addition, the continuous distortion of the lattice, analogous to that discussed in the previous subsection, should appear below H_{FL} in all vortex structures, because of the different scaling parameters s for each component. Such an anomalous field dependence of the angle α was observed by Kleiman *et al.*[22] at $T=50$ mK for $\mathbf{H}\perp c$. The prediction in our model of the distorted hexagonal lattice with the long triangle side along the z axis for $H_1>H_0$ coincides with their experimental observation. Moreover, the angle α is predicted to be $\tan^2\alpha=1/3(1+C)$, that is, $\alpha\approx 21°$, which is quite close to the experimental value. However, we do not try to fit their results as the experimental errors in the most interesting range of fields near H_{c2} are too large.

C. Comparison with experiment

To compare the calculated lines of phase transitions inside a mixed state with experimental data,[44] one needs to know the additional phenomenological parameter β_2/β_1. Using Eq. (8) we estimate it from the experimental value of T_c^- as $\beta_2=0.233\beta_1$. The corresponding phase boundaries for $\mathbf{H}\perp c$ and $\mathbf{H}\|c$ are plotted in Figs. 4(a) and 4(b). While the transition line $H_{FL}(T)$ at $T>T_k$ (the AB boundary in standard notations) is fitted quite well for both directions, there is a significant discrepancy between experimental and calculated slopes of $H_{FL}(T)$ at $T<T_k$ (the BC phase boundary). Note that the same discrepancy was found in the framework of the AB and SBF models.[8,12] In order to fit the BC phase boundary for $\mathbf{H}\perp c$, an additional diamagnetic term of the form $|\mathbf{H}\cdot\boldsymbol{\eta}|^2$ was assumed for the E_{1u} order parameter in Ref. 12. However, this explanation seems to be doubtful because the same discrepancy between theoretical and experimental transition lines exists also for $\mathbf{H}\|c$, where this term does not work.

In addition to ultrasonic data, we have fitted also the phase diagram of UPt_3 obtained from dilatometry[46] and magnetocaloric[47] measurements. The derived parameters are given in Table I. Again three phase boundaries are fitted rather well, while the experimental BC line lies always below the calculated curve.

In a tilted magnetic field all three components of the order parameter appear simultaneously at the upper critical field. This, however, does not necessarily mean the disappearance of the phase transition in the vortex lattice below H_{c2}. If the nonzero displacement is energetically preferable, the corresponding breaking of translational symmetry should occur as a phase transition even in the absence of rotational symmetry about $\mathbf{H}$.

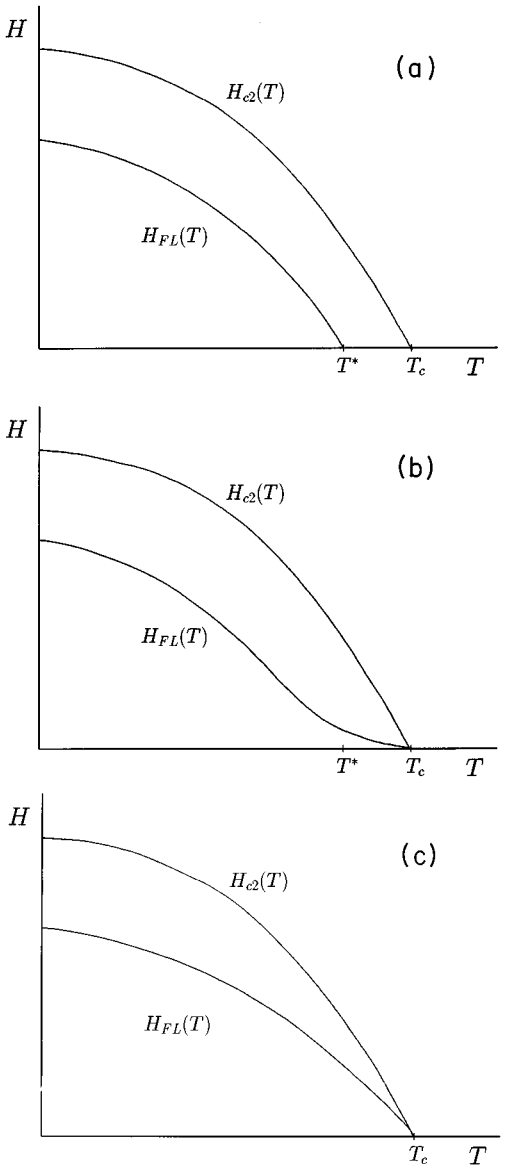

FIG. 7. Different types of the phase diagram of UPt_3 at pressures above the critical value: (a) in the AB model, arbitrary direction of field, and in the AE model, $\mathbf{H}\|c$; (b) in the AE model, $\mathbf{H}\perp c$; and (c) in the E_{1g} model, arbitrary direction of field.

D. Magnetic phase diagram at high pressures

If a magnetic field is applied parallel to the c axis, the phase diagrams are identical for the AE and AB models. The tetracritical point in the H-T plane, which exists at $P<P_{cr}$, shifts to lower fields and higher temperatures with increasing pressure and disappears at $P=P_{cr}$. After that the phase diagram consists of two smooth nonintersecting lines $H_{c2}(T)$ and $H_{FL}(T)$ as shown schematically in Fig. 7(a). The extrapolated temperature, at which the curve $H_{FL}(T)$ crosses the $H=0$ axis, is given by

$$T^*=\frac{T_0\delta_1-T_1\delta_{\rm int}}{\delta_1-\delta_{\rm int}}. \tag{41}$$

By replacing spatial averages in expressions for δ_1 and $\delta_{\rm int}$ by 1 in a low-field region, it can be shown that T^* coincides with the expression for T_c^- in the AB model ($P>P_{\rm cr}$) and with the expression for the temperature of the second transition (14) in the AE model if the small parameter β_3 is taken into account in (32)–(34). This confirms the previous assumption[16] that the extrapolation of the $H_{FL}(T)$ curve may be used to determine position of the fourth transition line in the P-T plane.

The same type of H-T diagram holds in the AB model when a magnetic field is applied in the basal plane. However, for the AE model the situation becomes more complicated. If $T_1>T_0$, the mixing of the η_y component to the eigenstate (23) cannot be neglected in the region $T_0<T<T_1$. This admixture leads to the upward curvature of $H_{FL}(T)$ which goes directly to T_c [Fig. 7(b)]. A further experimental investigation of the H-T diagrams for $\mathbf{H}\|c$ and $\mathbf{H}\perp c$ is needed in order to choose between the two accidental degeneracy models.

As for the SBF models, the magnetic diagram at high pressures is expected to be different for models without mixing gradient terms[11–14] and for the recent proposal by Park and Joynt.[15] For the latter the phase diagram is the same as for a perfect hexagonal two-component superconductor,[26,30] which is shown in Fig. 7(c). On the other hand, SBF is used in the former models not only to split T_c, but also to change coefficients in gradient terms. This is necessary in order to have different slopes of critical fields in the absence of mixing gradient terms. Therefore, when the SBF disappears, the two first solutions of the linearized GL equations for a given direction of $\mathbf{H}$ have exactly the same critical fields near T_c. Even in the absence of the SBF the diamagnetic term $|\mathbf{H}\cdot\boldsymbol{\eta}|^2$ may again split critical fields for $\mathbf{H}$ directed in the basal plane. But for $\mathbf{H}\|\mathbf{c}$ all these models predict that the BC transition line and the $H_{c2}(T)$ curve merge. This conclusion can be modified, in principle, by turning on mixing gradient terms. For example, in the E_{2u} model such terms are possible for a noncylindrical Fermi surface.[11] However, the splitting of the critical fields produced by the additional gradient terms at $P>P_{\rm cr}$ is of the order of a splitting of the tetracritical point at $P=0$ and should be very small. The resulting phase diagram of the E_{1u} and E_{2u} scenarios with merging transition lines is in a sharp contrast with the earlier thermal expansion measurements,[46] which yield faster suppression of the BC transition than of the $H_{c2}(T)$ curve at $P\neq 0$, as well as with a recent direct observation of the inner transition line for $\mathbf{H}\|c$ by means of an ultrasonic technique.[16] Thus, we conclude that among different SBF models only the recent proposal of the E_{1g} order parameter by Park and Joynt[15] could satisfy, in principle, the H-T diagram of UPt_3 at $P>P_{\rm cr}$ for $\mathbf{H}\|c$, provided a more careful experimental study will show the phase diagram like in Fig. 7(c) in contrast to the observation by Boukhny *et al.*[16]

VI. DISCUSSION

To summarize, we have studied the phase diagram of UPt_3 in the model with two nearly degenerate order parameters corresponding to the A_1 and E_1 irreducible representations under the assumption of a weak effect of the crystal lattice on superconductivity. We have reproduced the well-known magnetic phase diagram with the tetracritical point in the H–T plane[44,46,47] and interpreted experimental results on the behavior of superconducting phases under pressure[16] and in a tilted magnetic field.[17]

An attractive feature of the AE model with weak-crystal-field effects in comparison with the other theories is a smaller number of phenomenological parameters which determine the form of the phase diagram. These two parameters C and β_2 not only give the tetracritical point in the H-T plane for $\mathbf{H}\|c$ and $\mathbf{H}\perp c$, but also reproduce roughly the anisotropy of the critical fields near T_c. Non-negligible effects on nonlinear and gradient terms in the GL functional (2) from the crystal lattice lead to additional parameters, which might explain the discrepancy between theory and experiment in the behavior of the BC phase boundary.

We have also discussed the features of the phase diagram of UPt_3 which can distinguish unambiguously between different types of superconducting order parameter and between different hypotheses of the T_c splitting. The key experiments include the following.

(i) Measurement of the phase diagram in a tilted field.[17] The existence of the tetracritical point is not affected by a change in the field direction for the E_{1u}, E_{2u}, and AB models. In contrast, a slight smearing is expected in the AE model (see Fig. 5). In the E_{1g} model such a smearing is most significant for $\mathbf{H}\|c$.

(ii) Measurement of the H-T phase diagram at pressures (strains) above the critical value after the disappearance of the T_c splitting. The behavior of the $H_{FL}(T)$ phase boundary for $\mathbf{H}\|c$ is different for the E_{1g} model on the one hand and the AB and AE models on the other hand. This line merges with the $H_{c2}(T)$ curve as P approaches $P_{\rm cr}$ in the E_{1u} and E_{2u} models.

(iii) The same for $\mathbf{H}\perp c$. The inner transition line behaves differently for the AB and AE models at a low-field region.

(iv) Zero-field properties of the superconducting phase at $P>P_{\rm cr}$ are also different in the AB and AE models. For the former the time-reversal symmetry is preserved, while for the latter, as well as for the SBF models, the time-reversal symmetry is broken directly below T_c. A corresponding effect can be observed, e.g., by muon spin resonance (μSR) measurements, which showed previously the existence of spontaneous magnetic moments in the low-temperature phase at $P=0$.[48]

(v) Observation of the vortex lattice below the $H_{FL}(T)$ transition line for $\mathbf{H}\|c$ by means of neutron diffraction scattering. The ''nontriangular'' forms of the flux lattice would support one of the two accidental degeneracy models.

As for the small sixfold modulation of H_{c2} for magnetic fields lying in the basal plane,[23] this feature may be interpreted in the considered model as an interaction of the E_1 components of the superconducting order parameter with the antiferromagnetic moments $|\mathbf{M}\cdot\boldsymbol{\eta}|^2$. In contrast to the SBF model,[14] we need not assume rotation of magnetic moments in the basal plane for this. Modulation of the upper critical field appears as a result of the interaction with the frozen domain structure $\mathbf{M}(\mathbf{r})$ with three types of antiferromagnetic domains.

ACKNOWLEDGMENTS

We are grateful to V. P. Mineev for useful discussions. This work was financially supported by the Grant-in-Aid from Ministry of Education, Science and Culture of Japan. M.E.Z. acknowledges also support from the International Science Foundation through Grant No. MGI000.

APPENDIX

Here we calculate the spatial averages for the interaction parameter (34). We use the standard procedure[45,42] which consists of a substitution of periodic solutions (35) into (34) and an integration over a large rectangle in the x-y plane ignoring boundary effects (see, e.g., Ref. 8 for more details). The interaction parameter is subdivided into two parts

$$\delta_{\rm int}=\delta_{\rm int}^{(1)}+\delta_{\rm int}^{(2)}, \tag{A1}$$

where $\delta_{\rm int}^{(1)}$ corresponds to the first two terms in (34), while $\delta_{\rm int}^{(2)}$ is the last phase-locking term. Measuring x_0 and y_0 components of the displacement between $f_0(\mathbf{r})$ and $\tilde{f}_0(\mathbf{r})$ in units of $b\cos\alpha$ and $b\sin\alpha$, respectively, we obtain

$$\delta_{\rm int}^{(1)}=\frac{\beta_1}{1+\omega^2}\sqrt{\sigma}\sum_{m,n}\cos[2\pi\rho m(n-x_0)]\times\exp\{-\pi\sigma[m^2+(n-y_0)^2]\}\times(1+\tfrac{1}{2}\omega^2\{\tfrac{3}{4}-\pi\sigma[m^2+(n-y_0)^2]+2\pi\sigma[m^2-(n-y_0)^2]+\pi^2\sigma^2[m^2-(n-y_0)^2]^2\}). \tag{A2}$$

Written in this form the parameter $\delta_{\rm int}^{(1)}$ possesses an explicit periodicity with respect to the elementary translations on **a** and **b**. Numerical evaluation of (A2) for two perfect triangular lattices with $\rho=\frac{1}{2}$ and $\sigma=\sqrt{3/2}$ gives $\delta_{\rm int}^{(1)}=1.153\beta_1$ for $x_0=y_0=0$ [the vortex structure in Fig. 6(a)]; $\delta_{\rm int}^{(1)}=0.862\beta_1$ for $x_0=1$, $y_0=0$ [Fig. 6(b)]; $\delta_{\rm int}^{(1)}=0.827\beta_1$ for $x_0=1$, $y_0=\frac{1}{3}$ [Fig. 6(c)].

The phase-locking term is nonzero only for the vortex structure with the second sublattice displaced on a half of a basis vector [Fig. 6(b)]:

$$\delta_{\rm int}^{(2)}=\frac{\beta_2\omega\cos(2\phi)}{1+\omega^2}\sqrt{2\sigma}\sum_{m,n}(-1)^{m+n}\cos(2\pi\rho mn)\times\exp[-\pi\sigma(m^2+n^2)][\pi\sigma(m-n)^2-\tfrac{1}{2}]. \tag{A3}$$

Calculation of the sum yields $\delta_{\rm int}^{(2)}=-0.089\beta_1$ and $\phi=\pi/2$. Thus, the minimal interaction energy $\delta_{\rm int}=0.774\beta_1$ and the highest critical field H_{FL} (30) are achieved for the two-quantum vortex lattice shown in Fig. 6(b).

[1] See L. Taillefer, J. Flouquet, and G. G. Lonzarich, Physica B **169**, 257 (1991); Z. Fisk and G. Aeppli, Science **260**, 38 (1993); H. v. Löhneysen, Physica B **197**, 551 (1994) for a review of experiments.

[2] R. Joynt, Supercond. Sci. Technol. **1**, 210 (1988).

[3] D. W. Hess, T. A. Tokuyasu, and J. A. Sauls, J. Phys. Condens. Matter **1**, 8135 (1989).

[4] K. Machida, M. Ozaki, and T. Ohmi, J. Phys. Soc. Jpn. **58**, 4116 (1989).

[5] E. I. Blount, C. M. Varma, and G. Aeppli, Phys. Rev. Lett. **64**, 3074 (1990).

[6] R. Joynt, V. P. Mineev, G. E. Volovik, and M. E. Zhitomirsky, Phys. Rev. B **42**, 2014 (1990).

[7] M. Ozaki and K. Machida, J. Phys. Soc. Jpn. **61** 1277 (1992).

[8] D.-C. Chen and A. Garg, Phys. Rev. Lett. **70**, 689 (1993); A. Garg and D.-C. Chen, Phys. Rev. B **49**, 479 (1994).

[9] V. P. Mineev, Pis'ma Zh. Éksp. Teor. Fiz. **57**, 659 (1993) [JETP Lett. **57**, 683 (1993)].

[10] M. E. Zhitomirsky and I. A. Luk'yanchuk, Pis'ma Zh. Éksp. Teor. Fiz. **58**, 127 (1993) [JETP Lett. **58**, 131 (1993)].

[11] J. A. Sauls, Adv. Phys. **43**, 113 (1994).

[12] Y. Hirano, T. Fujita, K. Machida, and T. Ohmi, J. Phys. Soc. Jpn. **64**, 210 (1995); K. Machida, T. Ohmi, and M. Ozaki, *ibid*. **64**, 1067 (1995).

[13] R. Heid, Ya. B. Bazaliy, V. Matisovits, and D. L. Cox, Phys. Rev. Lett. **74**, 2571 (1995).

[14] D. F. Agterberg and M. B. Walker, Phys. Rev. B **51**, 8481 (1995).

[15] K. A. Park and R. Joynt, Phys. Rev. Lett. **74**, 4734 (1995).

[16] M. Boukhny, G. L. Bullock, B. S. Shivaram, and D. G. Hinks, Phys. Rev. Lett. **73**, 1707 (1994); M. Boukhny, G. L. Bullock, and B. S. Shivaram, Phys. Rev. B **50**, 8985 (1994).

[17] S.-W. Lin, C. Jin, H. Zhang, J. B. Ketterson, D. M. Lee, D. G. Hinks, M. Levy, and B. K. Sarma, Phys. Rev. B **49**, 10 001 (1994).

[18] G. Aeppli *et al.*, Phys. Rev. Lett. **60**, 615 (1988); **63**, 676 (1989).

[19] P. A. Midgley, S. M. Hayden, L. Taillefer, B. Bogenberger, and H. v. Löhneysen, Phys. Rev. Lett. **70**, 678 (1993).

[20] S. M. Hayden, L. Taillefer, C. Vettier, and J. Flouquet, Phys. Rev. B **46**, 8675 (1992).

[21] T. Trappmann, H. v. Löhneysen, and L. Taillefer, Phys. Rev. B **43**, 13 714 (1991).

[22] R. N. Kleiman *et al.*, Phys. Rev. Lett. **69**, 3120 (1992).

[23] A small hexagonal anisotropy in H_{c2} was detected by N. Keller, J. L. Tholence, A. Huxley, and J. Flouquet, Phys. Rev. Lett. **73**, 2364 (1994).

[24] E. D. Isaacs *et al.*, Phys. Rev. Lett. **75**, 1178 (1995).

[25] S. K. Yip, T. Li, and P. Kumar, Phys. Rev. B **43**, 2742 (1991).

[26] T. A. Tokuyasu, D. W. Hess, and J. A. Sauls, Phys. Rev. B **41**, 8891 (1990).

[27] T. A. Tokuyasu and J. A. Sauls, Physica B **165&166**, 347 (1990).

[28] K. Machida, T. Fujita, and T. Ohmi, J. Phys. Soc. Jpn. **62**, 680 (1993).

[29] R. Joynt, Europhys. Lett. **16**, 289 (1991).

[30] M. E. Zhitomirsky and I. A. Luk'yanchuk, Zh. Éksp. Teor. Fiz. **101**, 1954 (1992) [Sov. Phys. JETP **74**, 1046 (1992)].

[31] R. Joynt, T. M. Rice, and K. Ueda, Phys. Rev. Lett. **56**, 1412 (1986); P. Kumar and P. Wölfle, *ibid*. **59**, 1954 (1987); M. Sigrist and T. M. Rice, Phys. Rev. B **39**, 2200 (1989); I. A. Luk'yanchuk and V. P. Mineev, Zh. Éksp. Teor. Fiz. **95**, 709 (1989) [Sov. Phys. JETP **68**, 402 (1989)].

[32] P. Coleman, Physica B **206&207**, 872 (1995).
[33] W. Putikka and R. Joynt, Phys. Rev. B **37**, 2372 (1988).
[34] M. R. Norman, Phys. Rev. B **39**, 7305 (1989).
[35] Y. Kohori *et al.*, J. Phys. Soc. Jpn. **57**, 395 (1988); G. M. Luke *et al.*, Phys. Lett. A **157**, 173 (1991).
[36] C. Choi and J. A. Sauls, Phys. Rev. Lett. **66**, 484 (1991).
[37] N. D. Mermin, Phys. Rev. A **9**, 868 (1974).
[38] G. E. Volovik and L. P. Gor'kov, Zh. Éksp. Teor. Fiz. **88**, 1412 (1985) [JETP **61**, 843 (1985)].
[39] M. Sigrist and K. Ueda, Rev. Mod. Phys. **63**, 239 (1991).
[40] L. P. Gor'kov, Sov. Sci. Rev. A **9**, 1 (1987); C. Choi and P. Muzikar, Phys. Rev. B **40**, 5144 (1989).
[41] M. E. Zhitomirsky, Pis'ma Zh. Éksp. Teor. Fiz. **49**, 333 (1989) [Sov. Phys. JETP Lett. **49**, 379 (1989)]; S. K. Sundaram and R. Joynt, Phys. Rev. B **40**, 8780 (1989).
[42] I. A. Luk'yanchuk and M. E. Zhitomirsky, Supercond. Rev. **1**, 207 (1995).
[43] V. G. Kogan and J. R. Clem, Phys. Rev. B **24**, 2497 (1981).
[44] S. Adenwalla *et al.*, Phys. Rev. Lett. **65**, 2298 (1990).
[45] D. Saint-James, G. Sarma, and E. J. Tomas, *Type II Superconductivity* (Pergamon, Oxford 1969).
[46] N. H. van Dijk, A. de Visser, J. J. M. Franse, S. Holtmeier, L. Taillefer, and J. Flouquet, Phys. Rev. B **48**, 1299 (1993); N. H. van Dijk, A. de Visser, J. J. M. Franse, and L. Taillefer, J. Low Temp. Phys. **93**, 101 (1993).
[47] B. Brogenberger, H. v. Löhneysen, T. Trappmann, and L. Taillefer, Physica B **185&186**, 248 (1993).
[48] G. M. Luke *et al.*, Phys. Rev. Lett. **71**, 1466 (1993).